Received: 3 May 2018 | Revised: 4 September 2018 | Accepted: 29 November 2018

DOI: 10.1002/prot.25638

WILEY PROTEINS

RESEARCH ARTICLE

Residue-level determinants of angiopoietin-2 interactions with its receptor Tie2

Anna Bakhman[1] | Eitan Rabinovich[2] | Tomer Shlamkovich[2] | Niv Papo[2] | Mickey Kosloff[1]

[1]Department of Human Biology, Faculty of Natural Sciences, University of Haifa, Haifa, Israel

[2]Department of Biotechnology Engineering and the National Institute of Biotechnology in the Negev, Ben-Gurion University of the Negev, Beer-Sheva, Israel

Correspondence
Mickey Kosloff, Department of Human Biology, Faculty of Natural Sciences, University of Haifa, Haifa, Israel.
Email: kosloff@sci.haifa.ac.il

Funding information
European Research Council "Ideas program" ERC-2013-StG , Grant/Award Number: 336041; Israel Ministry of Science, Technology and Space, Israel, and the Italian Ministry of Foreign Affairs, Grant/Award Number: 3-10704; Israel Science Foundation, Grant/Award Number: 1454/13, 1959/13, 2155/15

Abstract

We combined computational and experimental methods to interrogate the binding determinants of angiopoietin-2 (Ang2) to its receptor tyrosine kinase (RTK) Tie2—a central signaling system in angiogenesis, inflammation, and tumorigenesis. We used physics-based electrostatic and surface-area calculations to identify the subset of interfacial Ang2 and Tie2 residues that can affect binding directly. Using random and site-directed mutagenesis and yeast surface display (YSD), we validated these predictions and identified additional Ang2 positions that affected receptor binding. We then used burial-based calculations to classify the larger set of Ang2 residues that are buried in the Ang2 core, whose mutations can perturb the Ang2 structure and thereby affect interactions with Tie2 indirectly. Our analysis showed that the Ang2-Tie2 interface is dominated by nonpolar contributions, with only three Ang2 and two Tie2 residues that contribute electrostatically to intermolecular interactions. Individual interfacial residues contributed only moderately to binding, suggesting that engineering of this interface will require multiple mutations to reach major effects. Conversely, substitutions in substantially buried Ang2 residues were more prevalent in our experimental screen, reduced binding substantially, and are therefore more likely to have a deleterious effect that might contribute to oncogenesis. Computational analysis of additional RTK-ligand complexes, c-Kit-SCF and M-CSF-c-FMS, and comparison to previous YSD results, further show the utility of our combined methodology.

KEYWORDS

high-throughput mutagenesis, protein-protein interactions, structural bioinformatics, tyrosine kinases

1 | INTRODUCTION

Angiopoietin-2 (Ang2) binding to its receptor Tie2 is a notable model system for protein-protein interactions in receptor tyrosine kinase (RTK) signaling. This system has significant biological and pharmaceutical importance, as it regulates central physiological processes such as angiogenesis and vascular permeability.[1–3] Nevertheless, wide knowledge gaps exist about Ang2-Tie2 interactions. For example, Ang2 can act either as an agonist or an antagonist of Tie2, depending upon their concentrations and the molecular context;[4–7] yet, the structural basis for this paradoxical function is unknown. Ang2 binding to Tie2 plays a central role in pathologies such as inflammation, autoimmune diseases, sepsis, ophthalmic diseases, developmental abnormalities, and tumorigenesis,[8–10] making this system an attractive drug target.[11] Indeed, anti-angiogenic therapies that center on the comparable RTK ligand VEGF are already in the clinic and more angiogenesis-targeted drugs are in development.[12,13] Different strategies have been explored to prevent Ang2 binding to Tie2 as potential therapies for ophthalmic diseases and for cancer.[9,14,15] Nevertheless, the molecular determinants of Ang2 binding to Tie2 are not fully understood at the individual amino acid level, impeding advances toward a therapeutic goal of re-engineering Ang2 into an effective antagonist.

Some molecular details of Ang2-Tie2 binding were revealed by previous structural studies.[16] Although both Ang2 and Tie2 are large proteins (around 500 and 1100 residues, respectively), the domains that are actually involved in binding are much smaller, encompassing

about 200 residues on either side.[6,17] Therefore, interactions between Ang2 and Tie2 are set by the compact Ang2 fibrinogen-like domain (Ang2-BD) that binds the Ig2 domain of Tie2, with negligible conformational changes in both domains.[17] Based on the crystal structure of monomeric Ang2, Barton et al. designed two Ang2 mutants that abolished binding to Tie2: the F469A/Y475A/Y476A triple mutant that simultaneously removed three large hydrophobic side chains at the center of the interface, and the K468E/K473E double mutant that introduced dual charge-reversals at the middle of the interface.[18] A subsequent crystal structure of the Ang2-BD-Tie2 complex[17] revealed that these residues are in the vicinity of the Ang2-Tie2 interface and suggested that three other Ang2 positions are also at the interface (N467, S480) or adjacent to it (S417) and might encode for receptor specificity across the paralogs of Ang2—Ang1, Ang3, and Ang4.[19,20] However, single-residue Ang2-BD mutants were not tested in previous studies, so the contributions and importance of individual Ang2 residues are not known. Moreover, the intrusive character of the K468E/K473E charge-reversal mutants that were tested by Barton et al. makes it difficult to gauge the particular role and importance of these charged residues in binding Tie2. Therefore, a more in-depth examination of individual residue contributions across Ang2-BD (both interfacial and buried) and their precise role in Tie2 binding can provide a better understanding of these interactions and guide the engineering of Ang2 variants as leads for drug development efforts.

More generally, identification of RTK ligand residues that influence protein-protein interactions, such as Ang2 binding to Tie2, is critical for understanding the biological role of these interactions and for designing better therapeutics. Toward this goal, it is useful to classify the effect of mutations in individual residues that affect protein-protein interactions into two categories: (1) Mutations of interfacial residues that participate in intermolecular interactions and thereby can affect these interactions directly or (2) mutations of noninterfacial residues that affect interactions indirectly, through intramolecular changes in the protein's tertiary structure, and thereby either destabilize the protein, affect its folding, or modulate its intermolecular interactions through allosteric effects via residues in the first category.[21–30]

Here, we used two different physics-based computational methodologies to interrogate the high-resolution (residue level) determinants of Ang2-BD binding to Tie2—both directly and indirectly, as defined above. We combined our computational predictions with random and site-directed mutagenesis and yeast surface display (YSD), an orthogonal method that has been used for the in vitro evolution of various proteins,[31–33] which identified specific substitutions in Ang2-BD that actually perturbed binding. This combination also provided insights into the use of high-throughput mutagenesis to interrogate the residue-level determinants of Ang2-Tie2 interactions. For a wider perspective, we also applied our computational methodologies to additional RTK-ligand complexes, showing our approach is generalizable to comparable complexes. The residue-level maps of RTK ligand binding determinants we provide can facilitate a more precise investigation of their biological and pathological roles and guide the development of protein-based therapeutics based on these protein ligands.

2 | MATERIALS AND METHODS

2.1 | Protein structures and sequences

We used the following three-dimensional (3D) structures in our analysis (with PDB codes): Ang2-Tie2 (2GY7),[17] SCF-c-Kit (2E9W),[34] murine CSF-FMS (3EJJ),[35] human CSF (5LXF).[36] In our calculations, we used the individual domains of the ligand and the receptor that form the actual ligand-receptor complex, based on visual inspection of the structures: Ang2 313-495 (Ang2-BD), Tie2 23-210, SCF 2-140, and CSF 4-148. 3D structural visualization and superimpositions were carried out with the molecular graphics program Pymol (http://pymol.org).

For comparison of Ang2 orthologs, we used sequences from the following organisms (NCBI RefSeq identifiers): *Homo sapiens* (NP_001138.1), *Macaca mulatta* (XP_001097949.1), *Equus caballus* (XP_005606481.1), *Canis lupus familiaris* (NP_001041591.1), *Bos taurus* (NP_001092325.1), *Alligator mississippiensis* (XP_006274905.1), *Gallus gallus* (XP_015140299.1), *Xenopus tropicalis* (OCA35262.1), and *Danio rerio* (NP_001265754.1); the following sequences from the OMA database (http://omabrowser.org/): *Pteropus vampyrus* (PTEVA07732), *Pseudotsuga sinensis* (PELSI14297), *Mus musculus* (AAB63189.1), *Lepisosteus oculatus* (LEPOC05406), *Gasterosteus aculeatus* (GASAC09912), *Oryzias latipes* (ORYLA05115), *Takifugu rubripes* (TAKRU18609), and *Tetraodon nigroviridis* (TETNG06190). For comparison of Tie2 orthologs, we used sequences from the following organisms (OMA identifiers): *H. sapiens* (HUMAN28579), *M. mulatta* (MACMU08729), *C. familiaris* (CANLF02222), *E. caballus* (HORSE11117), *B. Taurus* (BOVIN18390), *Choloepus hoffmanni* (CHOHO10231), *M. musculus* (MOUSE15977), *P. vampyrus* (PTEVA09829), *G. gallus* (CHICK14394), *P. sinensis* (PELSI09146), *Anolis carolinensis* (ANOCA02431), *X. tropicalis* (XENTR04291), *Latimeria chalumnae* (LATCH07960), and *D. rerio* (DANRE21150). Sequences were aligned using MAFFT (http://mafft.cbrc.jp/alignment/software/) and visualized using Boxshade (http://www.ch.embnet.org/software/BOX_form.html).

2.2 | Energy calculations to identify residues that contribute directly to protein-protein interactions

We followed the methodology described previously[32,36–40] to analyze the per-residue contributions of Ang2 and Tie2 residues to intermolecular interactions in the complex (Supporting Information Figure S1). The finite difference Poisson-Boltzmann (FDPB) method[41] was used to calculate the net electrostatic and polar contributions ($\Delta\Delta G_{elec}$) of each residue that is within 15 Å of the dimer interface. Residues that contributed substantially to the interaction were defined as those contributing $\Delta\Delta G_{elec} \geq 1$ kcal/mol to the interactions (twice the maximal numerical error of the electrostatic calculations).[37,42] Nonpolar energy contributions ($\Delta\Delta G_{np}$) were calculated as a surface-area proportional term, by multiplying the per-residue surface area buried upon complex formation, calculated using surfv,[43] by a surface tension constant of 0.05 kcal/mol/Å^2.[42] Residues that contributed substantially to binding were defined as those contributing $\Delta\Delta G_{np} \geq 0.5$ kcal/mol to the interactions (namely, bury more than 10 Å^2 of each protein surface upon complex formation). FoldX calculations were performed

using the AlaScan function as follows: with the Ang2-BD-Tie2 complex, to identify Ang2 residues that contribute directly to interactions with Tie2, and with the Ang2-BD monomer, to identify residues that upon mutation can destabilize the monomer and thereby affect interactions with Tie2 indirectly.[44] Following Tokuriki et al., residues with $\Delta\Delta G$ value >0 were predicted to impair interactions.[45]

2.3 | Burial-based classification of residues

To classify residues that can affect the tertiary structure of a protein, we measured the accessible surface area (ASA) of each residue using surfv.[43] We then calculated the relative accessible surface area (rASA) for each residue by dividing its ASA value by the maximal empirical ASA for each residue. The latter was taken from the empirical values calculated for each amino acid from a large dataset of structures culled from the PDB by Tien et al.,[46] who followed the approaches laid out by Rose et al.[47] and Miller et al.[48] Buried surface area (BSA) was calculated by subtracting the ASA of each residue from the maximal empirical ASA value for that residue (see above). We classified a residue as "core" if it had a rASA ≤5% or BSA ≥ 200 Å^2. The latter term was found to be applicable only to the following large residues: arginines, lysines, phenylalanines, tyrosines, and tryptophans. We classified a residue as "buried" if it had 5% > rASA ≤15%.

2.4 | YSD and Ang2-Tie2 binding measurements

YSD library construction and affinity measurements were performed similarly to previous works (Supporting Information Figure S2).[32,33,36] The Ang2 wild-type binding domain gene (*Ang2-BD$_{WT}$*) was introduced into *Saccharomyces cerevisiae* EBY100 yeast strain (generously provided by Amir Aharoni, Ben-Gurion University of the Negev, Israel) using the YSD pCTCON20 vector (generously provided by the Wittrup laboratory, MIT). The Ang2-BD$_{WT}$ protein (positions 281-496) was thus displayed on the yeast cell surface conjugated to a c-Myc tag by a linker (LPDKPLAFQDPS) at the C-terminus and to an HA tag at the N-terminus (Supporting Information Figure S2). To verify expression and correct folding of the YSD Ang2-BD$_{WT}$ construct, we incubated yeast cells expressing Ang2-BD$_{WT}$ with the soluble Tie2 receptor (positions 23-745) conjugated to an Fc domain (50 nM), monitoring protein expression and protein binding with FACS using fluorescent labeling with an anti-c-Myc antibody and an anti-Fc antibody, respectively.

For random mutagenesis, Ang2-BD$_{wt}$ was cloned into the pCTCON20 backbone plasmid (linearized by the NheI and BamHI restriction enzymes) by homologous recombination via electroporation into the EBY100 yeast strain using the Gene Pulser Transfection Apparatus (Bio-Rad, CA). Prior to homologous recombination, Ang2-BD$_{wt}$ was elongated using primers with a pCTCON20 plasmid homology sequence, NheI, and BamHI restriction sites, and a linker (TTGCCAGATAA ACCATTGGCTTTCCAAGATCCATCT) located between the 3′ end of Ang2-BD$_{wt}$ gene and the 5′ end of an c-Myc tag (Supporting Information Figure S2). The Ang2 random mutagenesis variant library was constructed by PCR with the GeneMorph II random mutagenesis kit (Stratagene, CA), according to the product protocol for a low mutation rate, using 750 ng of Ang2-BD$_{WT}$ DNA as template, and amplified using Phusion HF DNA polymerase (New England Biolabs, MA) to reach 5 μg of DNA. The resulting library was cloned into the pCT plasmid as described above and grown on SD-CAA plates (0.54% disodium phosphate w/v, 0.856% monosodium phosphate monohydrate w/v, 18.2% sorbitol, 1.5% agar, 2% dextrose, 0.67% yeast nitrogen base w/v, 0.5% bacto-casamino acids w/v), with serial dilution plating for library size determination, resulting in 6.1×10^5 individual clones. Library diversity was verified by sequencing 15 random colonies. The transformed Ang2-BD$_{wt}$ and the Ang2-BD library were incubated in SD-CAA medium at 30°C, with shaking at 300 rpm overnight until OD$_{600}$ of 10 (10^8 cells/ml) was reached and stored at 4°C.

Designed Ang2-BD mutants were generated as above, except that all the mutant gene sequences were generated by Hy Laboratories (Hylabs, Israel) based on the pCT-Ang2-BD$_{WT}$ plasmid construct. YSD constructs were induced in galactose-containing SG-CAA medium (2% galactose w/v, 0.67% yeast nitrogen base w/v, 0.5% bacto casamino acids w/v, 1.47% sodium citrate w/v, and 0.429% citric acid monohydrate w/v) at 30°C, with shaking at 300 rpm until OD$_{600}$ of 5 was reached. The expressed YSD library was fluorescently labeled as follows: about 1×10^6 cells from the SG-CAA medium were washed with Tie2 binding buffer [10 mM Hepes pH 7.0, 150 mM NaCl and 1% bovine serum albumin (BSA) in phosphate buffered saline] and then incubated with recombinant human Tie2-Fc chimera (R&D Systems MN) and an anti-c-Myc antibody (9E10, Abcam, MA) in Tie2 binding buffer for 1 hour at room temperature. The cells were then washed with ice-cold Tie2 binding buffer and incubated with anti-mouse IgG-PE antibody (Sigma, MO) and anti-human IgG (Fc specific) FITC antibody (Sigma) in Tie2 binding buffer at 4°C for 20 minutes in the dark. Cells were washed again with ice-cold Tie2 binding buffer and resuspended in 400 μL of Tie2 binding buffer for flow-cytometry analysis. To remove Ang2-BD clones that contain a stop codon or deletions/insertions, we performed a first sort in which we isolated Ang2-BD clones with a high expression level, and these were used in the following screening against soluble Tie2.

To measure Ang2 variant binding to Tie2 using FACS, the YSD Ang2 library was labeled with a soluble fluorescently labeled Tie2. To identify Ang2 variants with impaired affinity to Tie2, Tie2 concentrations were increased from 100 nM in the first screening cycle to 500 nM in the second cycle. Ang2 YSD expression levels were determined according to detection of c-Myc (Supporting Information Figure S2). Low-affinity Ang2 variant sorting was performed using geometrical sorting gates as shown in Supporting Information Figure S3 to overcome avidity effects, using the FACS Aria III (BD Biosciences, CA) or SY3200 (Sony Biotechnology Inc, CA). Each sorting step was analyzed by labeling Ang2 variants as in the screening step, using an Accuri C6 flow cytometer (BD Biosciences, CA) and FlowJo software (Treestar, Inc., CA). To identify single-point mutations that led to substantial Ang2 affinity reduction to Tie2, we collected variants at substantially reduced affinity (Supporting Information Figure S3). Binding measurements to Tie2 were performed as follows: yeast cells were induced and labeled as described earlier using 50 nM soluble Tie2 and an anti c-Myc antibody and fluorescently labeled secondary antibodies and analyzed in three independent repetitions as described earlier. The geometric mean of the affinity to Tie2 of each variant was normalized to its own geometric mean of expression,

and the results were normalized to Ang2-BD_{WT}/Tie2 binding results. SD error was calculated based on three independent replications for each sample.

3 | RESULTS

3.1 | Energy-based identification of Ang2 and Tie2 residues that contribute directly to Ang2-Tie2 interactions

To identify which individual residues are involved directly in Ang2-Tie2 binding (ie, are substantial contributors to Ang2-Tie2 binding), we analyzed the structure of Ang2-BD in complex with the Tie2 ligand-binding region using an energy-based approach. As the binding of Ang2 to Tie2 is set exclusively by Ang2-BD, we used these terms interchangeably here but performed analysis on Ang2-BD exclusively. There are many residues in the vicinity of the Ang2-Tie2 interface that can potentially contribute directly to Ang2-Tie2 interactions. For example, 53 of the 183 residues in the Ang2-BD and 42 of the 188 residues in the Tie2 ligand-binding domain are within 10 Å of the Ang2-Tie2 interface. To pinpoint the subset of Ang2 residues that actually contribute to interactions with Tie2 directly, we followed the approach we developed in previous studies.[32,36,37] We applied the FDPB method[41] to calculate the net electrostatic and polar contributions ($\Delta\Delta G_{elec}$) of each Ang2 and Tie2 residue that is within 15 Å of the binding partner. Note that our approach calculates the difference between the interactions of a residue with its protein partner in relation to its interaction with the solvent (see section 2.2) and thereby pinpoints only residues that are calculated to substantially contribute to binding. Nonpolar/hydrophobic energy contributions ($\Delta\Delta G_{np}$) were calculated as a surface-area proportional term by multiplying the per-residue surface area buried upon complex formation by a surface tension constant of 0.05 kcal/mol/Å^2.[37,42] Following previous work,[32,36] we defined residues that contribute significantly to interactions as those contributing $\Delta\Delta G_{elec} \geq 1$ kcal/mol to the interactions (twice the numerical error of the electrostatic calculations) or $\Delta\Delta G_{np} \geq 0.5$ kcal/mol to the interactions (namely, residues with more than 10 Å^2 of protein surface buried upon complex formation).

This analysis identified 15 Ang2 residues (6.5% of Ang2-BD) that contribute significantly to Tie2 binding (Table 1, Figure 1A and Supporting Information Figure S1). These residues are located in groups of two or three amino-acids, interspaced along a 50 residue stretch of Ang2. Only three of these residues were calculated to significantly contribute electrostatically to Tie2 binding via their side-chains, whereas the other 12 amino acids contribute only via nonpolar contributions. On the other side of the interface, we identified 12 Tie2 residues (8% of the Tie2 binding domain) that contribute significantly to Ang2-Tie2 interactions (Table 2). Nine of these contributing amino-acids originate from two adjacent groups of Tie2 residues, whereas the other three residues are interspaced further along the Tie2 molecule (Figure 1B). Two of these amino acids contribute electrostatically via their side-chains, whereas the other 10 residues make nonpolar contributions only. The residues that contribute electrostatically are located in two separate locations on each side of the interface (Figure 1C). Further inspection showed that Ang2-D448 and Tie2-R167 form a salt bridge, whereas Ang2-K473 and Ang2-S480 form a hydrogen bond network with Tie2-S164 (Figure 1D).

TABLE 1 Per-residue Ang2 energy contributions to direct interactions with Tie2

Ang2 residue	Energy contribution to interaction with Tie2
C433	np
I434	np
C435	np
M440	np
D448	np + elec
A449	np
C450	np
P452	np
N467	np
F469	np
K473	Elec
Y475	np
Y476	np
S480	np + elec
G481	np

Abbreviations: np: nonpolar; elec: side-chain electrostatic contribution.

3.2 | Experimental validation of Ang2 residues that affect Tie2 binding directly by directed alanine mutagenesis

We validated our predictions for residues that were calculated to contribute directly to interactions with Tie2 using site-directed alanine mutagenesis. We expressed Ang2 mutants using YSD and quantified the interactions of these variants with the soluble Tie2 extracellular domain using FACS (see Supporting Information Figure S2 and Methods for details). Ang2 expression was monitored by the conjugated c-Myc tag, and binding of Ang2 mutants to Tie2 was measured using soluble fluorescently labeled Tie2.

These experimental measurements show that, except for N467, single mutations in Ang2 residues that were computationally predicted to make direct electrostatic or nonpolar contributions to Tie2 all reduced binding (Figure 2). Combining these mutations in directly contributing residues into double and triple mutants reduced the affinity further, to < 25% of the wild-type protein. In particular, the F469A/Y475A/Y476A triple mutant, which was shown using qualitative gel filtration analysis to impair Tie2 binding,[18] reduced Tie2 binding by ~90%. Conversely, mutations in Ang2 residues in the vicinity of the Ang2-Tie2 interface that were not predicted to contribute to interactions with Tie2 directly did not show a dramatic change in binding. Although we did observe a reduction in the affinity of the K468A mutant, a double mutant with the K432A mutation showed no reduction in affinity. However, it is possible that the K432A mutation complements the K468A mutant, yet, the two residues are peripheral and on opposite sides of the interface, suggesting the reduction in affinity of the K468A mutant is not due to a specific direct effect on interactions with Tie2. These results differ from the affinity reduction

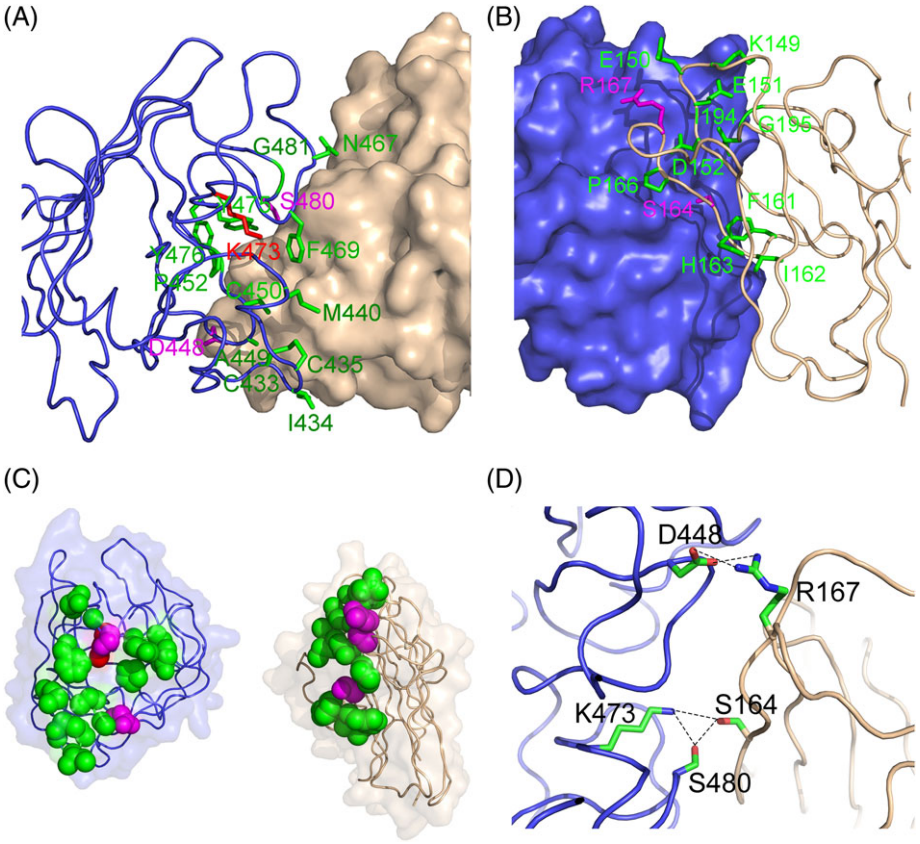

FIGURE 1 Ang2 and Tie2 residues that contribute significantly to direct interactions across the Ang2-Tie2 interface. A, Residues in Ang2 (blue ribbon) that contribute significantly to interactions with Tie2 (wheat molecular surface), shown as sticks and colored green (nonpolar contributions), red (side-chain electrostatic contribution), and magenta (nonpolar and side-chain electrostatic contributions). B, Residues in Tie2 (wheat ribbon) that contribute significantly to interactions with Ang2 (blue molecular surface), shown as sticks and colored as in A, rotated 180° about the x-axis relative to A. C, Ang2 and Tie2 residues that contribute significantly to Ang2-Tie2 interactions, shown as spheres and colored as in A and B. Ang2 and Tie2 are shown in an "open book" view, with Ang2 rotated 135° about the y-axis relative to A and Tie2 rotated 180° about the Y axis relative to Ang2. D, Ang2 and Tie2 residues that contribute to intermolecular interactions via electrostatic contributions (marked with dashed lines)

observed using qualitative gel filtration analysis for the more intrusive charge-reversal K468E/K473E double mutant.[18] Taken together, the site-specific alanine mutagenesis results show that the seven representative residues tested here, which we predicted contribute substantially to Tie2 binding, indeed play a role in this interaction. However, the additive nature of the YSD results suggests that none of these residues is absolutely necessary for measurable binding.

3.3 | Identification of Ang2 residues that affect Tie2 binding using random mutagenesis and YSD

To search in an unbiased way for individual substitutions that substantially reduce Ang2 binding, we used YSD and randomly inserted point mutations into Ang2 with error-prone PCR, aiming to incorporating on average one mutation per variant, generating a random library with 6.1×10^5 individual clones. We monitored the expression of these variants with the soluble Tie2 using FACS and quantified their interactions with soluble Tie2 as above. To remove Ang2-BD clones that contain a stop codon, deletions, or insertions we performed an initial sort for Ang2 clones with a high expression level. These variants were then screened against Tie2 to further select Ang2 variants with reduced affinity to Tie2 (Supporting Information Figure S3). The sorted library fraction (Supporting Information Figure S3C) was then incubated with a higher Tie2 concentration (500 nM) to identify point mutations in Ang2 that led to a substantial reduction in affinity in comparison to Ang2-BD wild type. We randomly selected 100 single

TABLE 2 Per-residue Tie2 energy contributions to direct interactions with Ang2

Tie2 residue	Energy contribution to interaction with Ang2
K149	np
E150	np
E151	np
D152	np
F161	np
I162	np
H163	np
S164	np + elec
P166	np
R167	np + elec
I194	np
G195	np

Abbreviations: np: nonpolar; elec: side-chain electrostatic contribution.

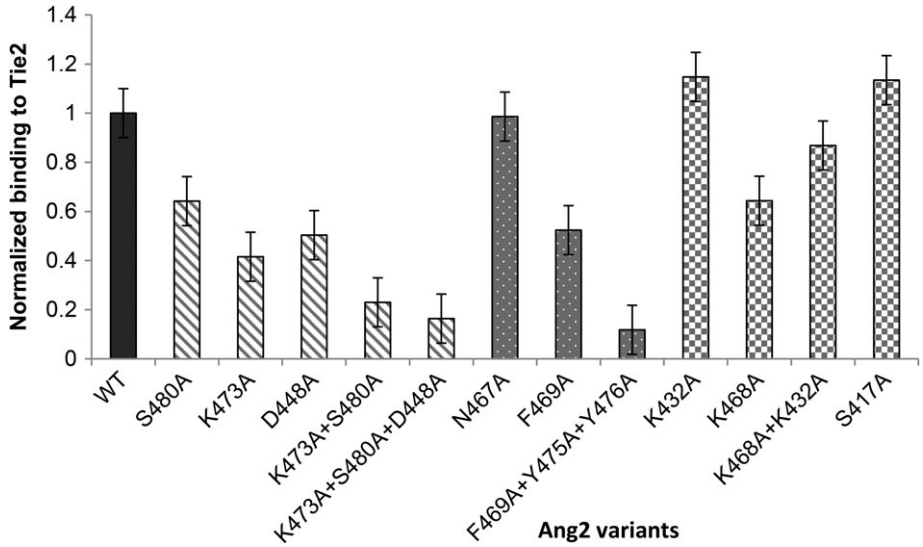

FIGURE 2 Mutations in Ang2 residues predicted to contribute substantially to interactions with Tie2 impair binding to Tie2 in an additive manner. Binding signals of individual Ang2 mutants, expressed on the yeast surface, to 50 nM soluble Tie2, normalized to their expression level and to the binding signal of Ang2-BD_{wt} (WT). Mutants were grouped according to the predicted structural role of the residues in their interactions with Tie2: residues that contribute electrostatically (striped), residues that make nonpolar contributions (dots), adjacent non-contributing residues (checkered). Each column value is a mean of triplicates ± s.e.m., $n = 3$

clones from this sorted library and sequenced them. This identified 12 different clones with a single amino acid mutation in Ang2-BD, whereas the rest of the sequences had multiple mutations. This frequency of single mutations converts into 73 200 single-nucleotide substitutions in our whole library, accounting for more than 10-fold the maximum theoretical diversity for single-nucleotide mutations in the Ang2-BD gene (the theoretical maximum is 1953 possible substituting mutations for a gene that has 651 bp),[32,49,50] thus spanning the entire sequence and residue substitution spaces for the Ang2-BD gene. All of the single amino acid mutations originated from a single nucleotide point mutation.

The 12 single-residue variants that substantially reduced Ang2-BD affinity to Tie2 had mutations in 11 different positions: W339R, N357S, S414L, S415N, N430S, D431N, T442I, A449V, N454D, N454S, K478N, and T487I. To quantify the reduction in affinity caused by each identified Ang2 mutation, we expressed each clone in the YSD setup and measured its affinity in the same concentration of Tie2 used above (50 nM) using FACS (Supporting Information Figure S3). As expected from our selection protocol (Supporting Information Figure S2), all of the point mutations we identified reduced affinity to Tie2 substantially, by ~70%-90% (Figure 3). Interestingly, out of the 11 positions substituted in these variants, only one Ang2 residue (A449) was identified in our energy-based calculations as making a direct (nonpolar) contribution to Tie2 interactions.

3.4 | Burial-based classification of Ang2 residues that can potentially affect its tertiary structure and thereby perturb interactions with Tie2 indirectly

We hypothesized that the Ang2 positions we identified above using random mutagenesis that were not predicted to contribute directly to Tie2 binding, affected binding indirectly. In particular, substitutions in residues that make up the core of a protein and thereby determine its tertiary structure can affect protein-protein interactions indirectly by perturbing the protein's folding and 3D conformation.[21,23,24,51] To identify such potential residues in Ang2, we sought to pinpoint which residues are either part of the protein's hydrophobic core or are buried enough so that a change in their physico-chemical properties will likely affect Ang2 interactions with Tie2 indirectly. To determine the burial of each Ang2 residue, we measured its ASA using surfv,[43] and then calculated the rASA for each residue by dividing the ASA value by the maximal empirical ASA for each residue (Supporting Information Figure S4A). Maximal empirical ASA values were taken from the empirical values calculated from the PDB by Tien et al.,[46] following the approaches of Rose et al.[47] and Miller et al.[48] We also calculated the buried surface area (BSA) values for each residue, as the difference between the maximal empirical ASA value and the calculated ASA for each residue (Supporting Information Figure S4B).

Instead of the more commonly used two-state classification of residues as "buried" or "exposed," following Rost and Sander.[52] we separated residues in the first category, which are substantially buried in the protein core, into the more informative classifications of "core" and "buried" residues. Accordingly, we classified all Ang2 residues into a three-state classification for residue burial: "core," "buried," and "exposed." Using the stringent threshold chosen by Refs. 47 and 48, residues with rASA ≤5% were classified as "core." Residues with 5% < rASA ≤15% were classified as "buried," and residues with rASA >15% were classified as "exposed" (Supporting Information Figure S5). However, we noticed that 12 of the largest Ang2 residues that were substantially buried, and based on visual inspection were part of the central protein core, had misleadingly high rASA values. All 12 of these residues (arginines, a lysine, a phenylalanine, tyrosines, and tryptophan) were large, yet had small ASA values and their BSA values were all above 200Å^2 (Supporting Information Figure S6). We therefore used the latter BSA value as an additional threshold to classify these residues also as "core," assuming such substantial burial can also

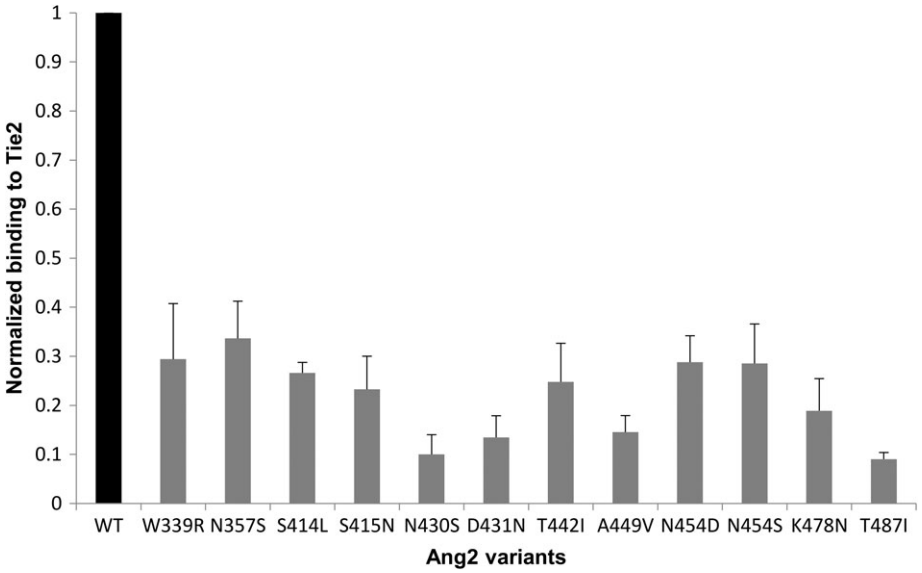

FIGURE 3 Ang2 variants selected for substantially lower Tie2 affinity using YSD. Binding signals of individual Ang2 variants (identified as in Supporting Information Figure S3) to 50 nM soluble Tie2 were normalized to their expression level and to the binding signal of Ang2-BD_{wt}. Binding values are mean ± s.e.m., $n = 3$

lead to considerable effects on protein structure upon mutation. Overall, 52 Ang2 residues were classified as "core" because they had rASA ≤5%, whereas 12 Ang2 residues were classified as "core" because they had BSA ≥ 200 Å^2. We note that some previous studies used much higher thresholds (eg, rASA ≤25%) to separate core and exposed residues,[51,53,54] but this would have led to over half of Ang2 being classified as core, reducing the utility of this classification. More importantly, such a lenient threshold would have classified almost a third of the directly contributing Ang2 residues as "core." Therefore, the more stringent thresholds we chose better separate residues that can potentially contribute to interactions directly versus indirectly.

According to this burial-based analysis, out of the 183 amino acids in Ang2, 64 residues were classified as "core" (Figure 4A), and 16 residues were classified as "buried" (Figure 4B). When combined together, the "core" and "buried" residues of Ang2 form a visibly compact part of the protein, which does not extend to the surface of Ang2 (Figure 4C). The 103 remaining residues were classified as "exposed" (Figure 4D). Our calculations therefore point to 80 core and buried Ang2 residues as positions that can potentially affect binding to Tie2 indirectly.

Indeed, most of the Ang2 residues we identified using random mutagenesis as impairing binding to Tie2 (Figure 3) were classified by our buried-based calculations as "core" or "buried" (Figure 5A). Five Ang2 residues were classified by us as "core" residues (W339, N357, S415, N454, and N487) and three Ang2 residues were classified as "buried" (S414, D431, T442). Two Ang2 residues (N430, K478) were not identified by either of computational approaches. However, a further structural analysis explained why mutations in these residues affected Tie2 binding. N430 is located in the middle of a calcium binding loop, which was shown to be important for the tertiary structure of Ang2 and thereby to Tie2 binding.[18] Therefore, the N430S mutation likely affected Tie2 binding indirectly by perturbing its tertiary structure and supports the previous suggestion that this loop is important for Tie2 binding. K478, on the other hand, is partially buried (~160 Å^2) and adjacent to K473 and S480, which are part of the electrostatic and hydrogen bond network to Tie2 S164 (Figure 5B). Therefore, the K478 N mutation likely impaired Tie2 binding indirectly by perturbed this hydrogen bond network. Both of these mutations exemplify a more intricate set of intramolecular interactions that nevertheless affect Tie2 binding indirectly. Overall, YSD pinpointed which variants actually impaired Ang2 affinity to Tie2, while our combined calculations provided a mechanistic explanation for these effects.

3.5 | Ang2 residues that affect interactions with Tie2 directly and indirectly are conserved across diverse organisms

To gain further insight into the functional importance of Ang2 residues that play either a direct or an indirect role in interactions with Tie2, we examined their conservation across representative organisms. We aligned 17 orthologous Ang2 sequences representative of all major vertebrate clades with MAFFT (see Methods) and saw that the majority of the directly contributing residues were conserved across all organisms (Supporting Information Figure S7). In particular, all residues that contributed electrostatically to interactions with Tie2 were identical across the alignment. Only three directly contributing positions (I434, M440, G481) showed some variability in fish. However, these residues contribute only nonpolar interactions, and the substitutions were mostly to residues with very similar physicochemical properties (eg, I434V and M440L). Importantly, all three of these positions were at the periphery of the Ang2-Tie2 interface and therefore presumably more tolerant to substitutions that will not affect the interface. Furthermore, almost all of the Ang2 residues we classified as "core" and most of the residues we classified as "buried" were also conserved across all Ang2 homologs. The few "core" or "buried" positions that showed some variability had very similar physicochemical properties as well.

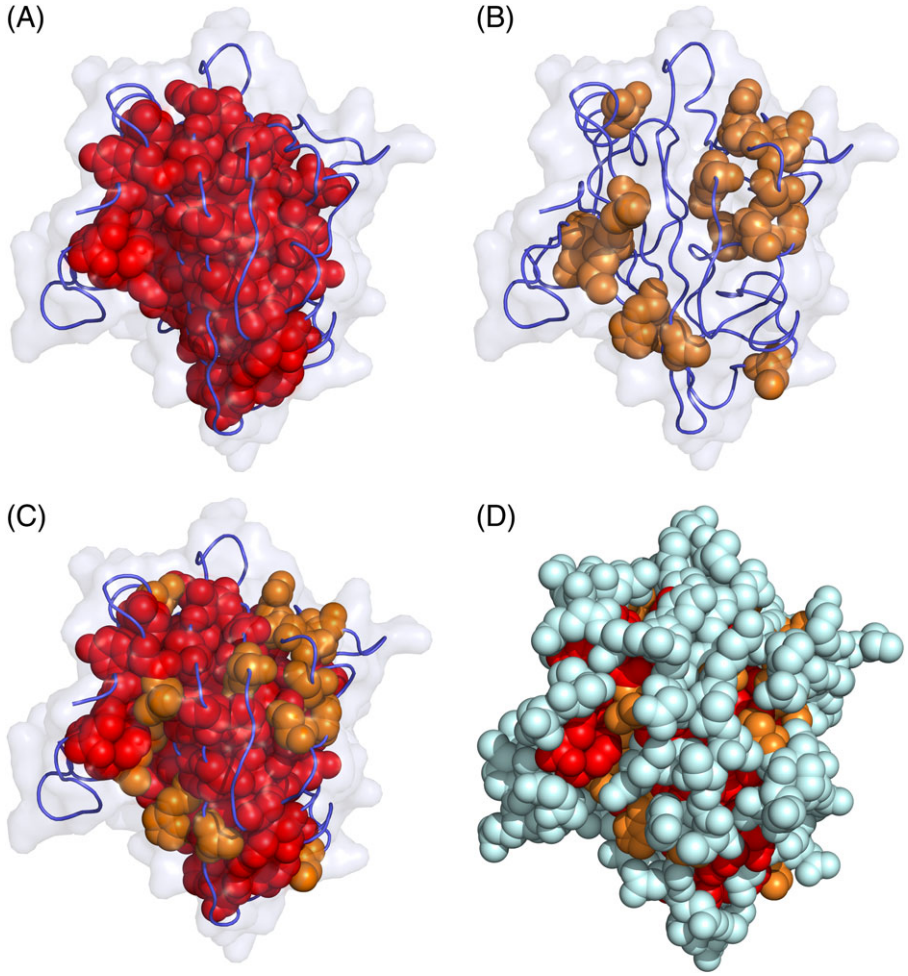

FIGURE 4 Ang2 positions that are classified as "core", "buried", and "exposed". A, The 64 Ang2 "core" residues (rASA ≤ 5% or BSA ≥ 200 Å^2) shown as red spheres. Ang2 is shown in blue tube representation, with transparent light gray molecular surface. B, The 16 "buried" Ang2 residues (5% < rASA ≤ 15%) shown as orange spheres, as in A. C, The 80 "core" and "buried" Ang2 residues shown together as in A and B. D, The 103 "exposed" Ang2 residues (rASA > 15%), shown as light cyan spheres, with the Ang2 core and buried residues shown as in C [Color figure can be viewed at wileyonlinelibrary.com]

A comparison of representative Tie2 orthologs showed a similarly high conservation (Supporting Information Figure S8). The two Tie2 residues that make both nonpolar and side-chain electrostatic contributions were conserved across all organisms. Almost all of the residues that make nonpolar contributions were conserved across all mammals and showed only limited variability in other organisms. Taken together, these results show that the residues we identified as important for Ang2-Tie2 interactions are all highly conserved across diverse vertebrates. This, in turn, suggests that the Ang2-Tie2 interface is highly conserved across diverse species.

3.6 | Comparison to predictions with alternative computational approaches

We compared our approach to other computational methods that can be used to predict residues that affect protein-protein interactions. We selected FoldX as a representative knowledge-based method to predict which Ang2-BD residue might affect Tie2 binding. We used the AlaScan function in FoldX (see Methods) to predict both residues that can affect intermolecular binding to Tie2 (direct contributions) and residues that can destabilize the Ang2-BD monomer (ie, affect interactions with Tie2 indirectly). Using a threshold of $\Delta\Delta G > 0$,[45] the first analysis predicted that out of 181 Ang2-BD residues, 132 residues (72%) have $\Delta\Delta G$ values above this threshold and therefore might perturb Tie2 binding by destabilizing intermolecular interactions in the Ang2-Tie2 complex (Supporting Information Figure S9A). Five of these residues were indeed shown by our directed mutagenesis (Figure 2) to impair binding to Tie2 (S480, D448, F469, Y475, Y476)—these residues were therefore predicted as direct contributors by both our energy-based calculations and by FoldX. N467 was predicted by both our calculations and FoldX to contribute to interactions, but alanine mutagenesis of this residue did not affect binding to Tie2. We note that the $\Delta\Delta G$ values that were predicted by FoldX for these experimentally-validated residues were small (usually <1 kcal/mol), so raising the threshold for significance (eg, to 1 kcal/mol, as in the Supporting Information Figure S1) would have led to most of these Tie2-interacting residues not to be predicted as such by FoldX, but dozens of other Ang2-BD residues with higher $\Delta\Delta G$ values would have remained as false-positives (Supporting Information Figures S9 cf. S1). Using an even more stringent threshold, such as the $\Delta\Delta G > 3$

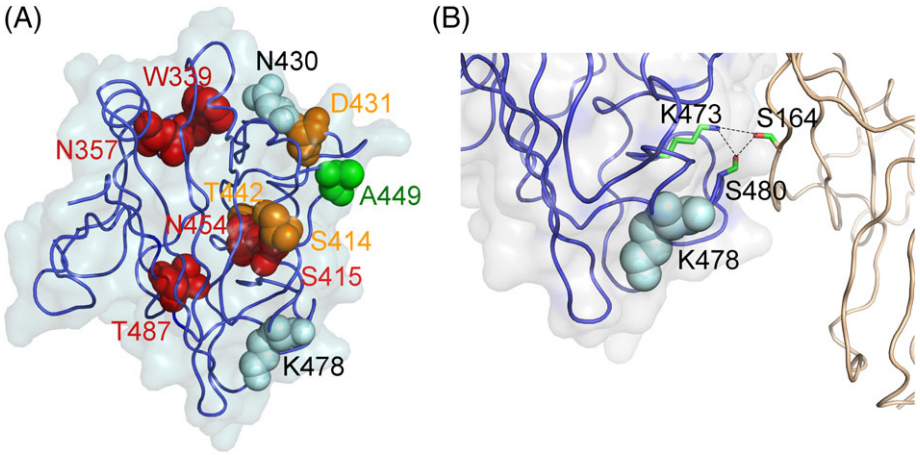

FIGURE 5 Predicted structural basis for Tie2 binding impairment by random Ang2 mutagenesis. A, The predicted structural classification of the Ang2 residues identified by random mutagenesis (Figure 3), shown as spheres. A directly contributing residue (green), five core residues (red), three buried residues (orange), and two "exposed" residues (light-cyan). Ang2 is shown in blue tube representation with transparent gray molecular surface. B, K478 is partially buried and is adjacent to the hydrogen bond network of Ang2-K473 and Ang2-S480 with Tie2-S164 (shown in sticks, as in Figure 1D) [Color figure can be viewed at wileyonlinelibrary.com]

threshold used in Ref. 51 for highly destablizing mutations, would have resulted in all Ang2 interface residues and the residues validated experimentally becoming false-negatives. Of particular interest is residue K473, which was predicted by our calculations to contribute electrostatically to interactions with Tie2 (Table 1); the directed mutagenesis of this Ang2-BD residue indeed reduced affinity to Tie2 (Figure 2). Contrastingly, FoldX predicted the K473A mutation will stabilize the Ang2-Tie2 complex. Interestingly, K473 was the only Ang2 residue predicted by our energy-based calculations to contribute favorably to interactions with Tie2 only via long-range electrostatic interactions, with no direct contributions via nonpolar interactions.

Analysis of FoldX predictions for the Ang2-BD monomer showed that a similar majority of Ang2-BD residues (133 of 181 residues, 74%) were predicted to destabilize the monomer (Supporting Information Figure S9B). Surprisingly, 6 of the 11 positions identified by our random mutagenesis to impair Tie2 binding were predicted by FoldX to stabilize the monomer, despite the fact that three of these were classified by our burial-based approach as core and two more were classified as buried. Overall, only 4 of the 11 Ang2 positions identified by our random mutagenesis as impairing Tie2 binding were predicted by FoldX to destabilize Ang2 or its complex with Tie2.

We also compared our approach to ISIS, a sequence-based method that predicts protein-protein interaction sites from local sequence information.[55,56] This method predicted that 26 of the 181 Ang2-BD residues contribute to protein-protein interactions (Supporting Information Table S1). Most of these residues are not in the vicinity of the Ang2-Tie2 interface. Only four of the positions predicted by ISIS were also classified by our energy-based analysis to contribute directly to interactions with Tie2 (M440, N467, F469, and Y476). Of these, alanine mutations in N467 did not impair affinity, whereas alanine mutations in F469 and Y476 did impair affinity (Figure 2). As expected, most of the residues predicted by ISIS were exposed, and only 4 of these 26 predicted residues were classified as "core." However, none of these predicted residues were identified by our random mutagenesis screen.

3.7 | Application of structure-based predictions to the RTK ligands SCF and M-CSF

For a wider biological and methodological perspective, we applied our approach to two more RTK ligands that belong to a different subfamily and were mutated in previous studies.[32,33] We used the two computational approaches detailed above on the structures of SCF with the c-Kit receptor, and of M-CSF with the c-FMS receptor and compared these computational predictions to previous random mutagenesis and YSD experimental results (Figure 6).

In SCF, there are 74 residues (out of 139) that are within 10 Å of the c-Kit receptor. Our calculations show that 29 SCF residues contribute directly to the interactions with c-Kit (Figure 6A). In total, 49 positions out of 139 SCF residues were classified as potentially affecting SCF interactions indirectly—35 were classified as "core" (25%), while 14 SCF residues (10%) were classified as "buried" (Figure 6C). Indeed, random mutagenesis and YSD identified 26 SCF variants with impaired binding to c-Kit, with almost all of these positions explained by our calculations: seven were in residues calculated to contribute to interactions with c-Kit directly (T9M, N10Y, N11K, K13T, S53L, D85N, E88K), nine were in residues classified as "core" (W44R, M48K, L56S, S71R, I76S, I82F, V83D, F115L, F119S), while three were in residues classified as "buried" (S55I, N72D, I123N). Seven variants that impaired binding to c-Kit were not in these predicted categories: A20T, N21K, D25E, Y26H, K62I, T111I, and E114K. However, the first five residues contribute directly to interaction across the SCF-SCF dimer interface via nonpolar contributions (A20, N21) and via electrostatic contributions (D25, Y26, K62). As perturbations of the ligand dimer interface were shown to reduce binding to c-Kit, this explains how these mutations affect ligand-receptor binding.[32] Therefore, YSD identified variants that affect binding through either interface, while the computational predictions enable to classify the source for the binding impairment in a transparent fashion. Only

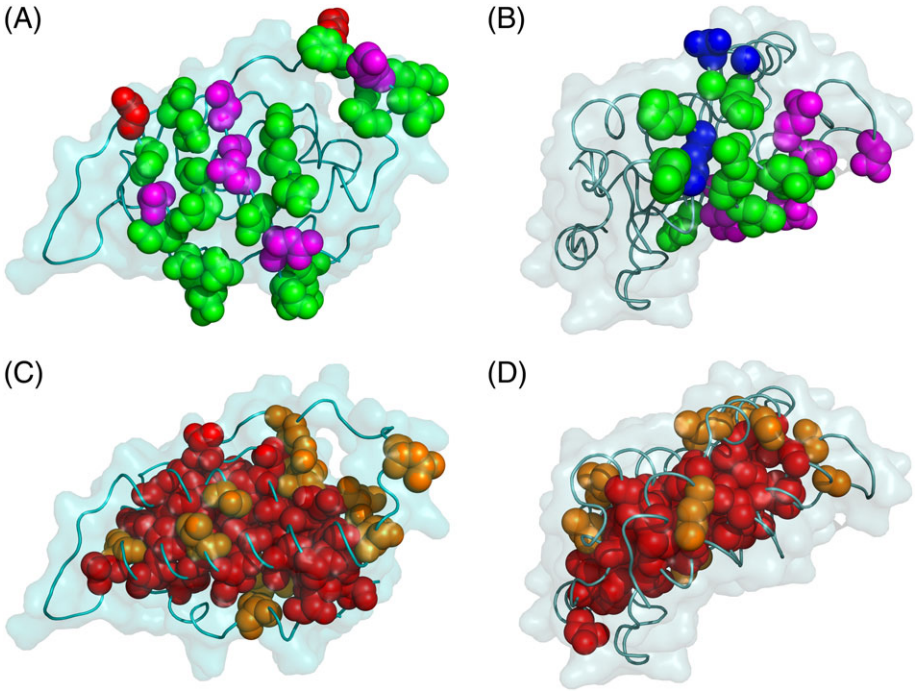

FIGURE 6 SCF and M-CSF residues that can affect interactions with their cognate receptors. A, SCF residues that contribute significantly to interactions with c-kit, shown as spheres and colored green (nonpolar contributions), red (side-chain electrostatic contribution) and magenta (nonpolar and side-chain electrostatic contributions). B, M-CSF residues that contribute significantly to interactions with c-FMS, shown as spheres and colored green (nonpolar contributions), blue (nonpolar and main-chain electrostatic contribution) and magenta (nonpolar and side-chain electrostatic contributions). C, The 35 SCF "core" residues, shown as red spheres, and 16 "buried" residues, shown as orange spheres. SCF is shown as a cyan ribbon with transparent molecular surface. D, The 40 M-CSF "core" residues and 11 "buried" residues, shown as in C [Color figure can be viewed at wileyonlinelibrary.com]

two positions identified by the random mutagenesis and YSD screening were not explicitly explained by our computational approach: T111 and E114. These two residues form an intramolecular hydrogen bond, and are packed against D25 and Y26, and presumably breaking this hydrogen bond affects SCF-SCF dimer formation and thereby indirectly impair binding to c-Kit. Including our predictions for residues that contribute directly to ligand dimerization, our computational approach provided a clear mechanistic explanation for binding impairment in 24 of the 26 SCF positions identified by the experimental screening.

In M-CSF, 64 of 144 M-CSF residues are within 10 Å of the cognate partner. We identified 19 M-CSF residues as direct contributors to c-FMS binding (Figure 6B), 40 M-CSF residues (28%) were classified as "core" and 11 residues (8%) were classified as "buried" (Figure 6D). On the other hand, YSD identified 40 variants in 33 positions that impaired M-CSF binding to c-FMS. About 13 variants were in 11 M-CSF positions that contributed directly to interactions with c-FMS (H9R, M10V, S13P, H15L, Q58R, D59G, V78A, Q79R, Q81R, E82G/A/K, L85S), 16 variants were in 13 positions classified as "core" (L19S, L22S, F35S/L, F37L, L43S, K52E, S84P, L87F, C90R, L114S, L128S, F135S, C139/Y/S), while two were classified as "buried" (D39G, C146S). Ten variants in seven positions, which impaired binding to c-FMS, were not in these predicted categories: S25P, Q26L/K/R, M27T, E28G/K, D45A, P72T, and I75T. Yet, similar to SCF, the first four of these M-CSF residues contribute directly to interaction across the M-CSF-M-CSF dimer interface via nonpolar contributions (E28) and via electrostatic contributions (S25, Q26, M27). Only three substitutions identified by the experimental screen were not explicitly explained by our calculations, but their effect can be explained by further structure analysis. D45 forms an intramolecular salt bridge within M-CSF. P72 is close to the dimer interface and presumably a mutation from a proline to a threonine will perturb its local tertiary structure, while I75 packs against P72, and a mutation in this residue might therefore also perturb the M-CSF dimer in a similar manner. Overall, our computational approach provided clear mechanistic explanations for 30 of the 33 M-CSF positions identified by the experimental screening. Therefore, our combined approach can both identify affinity-impairing variants and provide a rapid and accurate classification for this impairment.

4 | DISCUSSION

We combined two separate physics-based calculations with random and site-directed mutagenesis and YSD to identify which Ang2 residues can affect interactions with Tie2 and classify whether these substitutions impaired binding directly or indirectly. Thereby, we differentiated between Ang2 residues that contribute to intermolecular ligand-receptor interactions and those that can affect the protein's tertiary structure. Our analysis showed that the Ang2-Tie2 interface is dominated by nonpolar contributions, with only three Ang2 and two Tie2 residues that contribute electrostatically to intermolecular interactions. Previous visual inspection of the Ang2-Tie2 complex had suggested that additional polar or charged Ang2 residues might

contribute to interactions with Tie2, such as K432, K468, and S417.[17] However, our calculations predicted these residues do not contribute significantly, and indeed our site-directed alanine mutagenesis supports these predictions. Furthermore, the participation of Ang2 residues in binding Tie2 was previously tested using intrusive charge-reversal mutations,[18] which make it difficult to gauge the mechanistic role and importance of Ang2 residues in binding Tie2. By mutating individual contributing Ang2 residues to alanines, we showed that each residue contributes to Tie2 binding only moderately. Therefore, engineering of this interface will likely require a combination of double or triple mutations to reach substantial effects.

A distinct advantage of our combined approach to study this protein complex is highlighted by the fact that mutagenesis of the classified core or buried Ang2 residues had a more dramatic effect on binding Tie2 than mutations in interface residues. These results support a widely held hypothesis—that a moderate loss of stability is frequently associated with loss of function, which can also lead to genetic-based diseases.[27] It is therefore noteworthy that, in this particular case, using only a high-throughput random mutagenesis experimental approach could have missed the bulk of the interfacial Ang2 residues that contribute to Tie2 binding directly. Future high-throughput experimental studies can overcome this potential pitfall by either performing a presort with a conformational/structural antibody or by using additional sorting gates to select variants that have different levels of affinity reduction.

Interestingly, mutations in 23 of the Ang2 residues that we predicted can affect binding were found in human tumors (Supporting Information Table S2); 21 of these positions were in core or buried positions. The number of relevant samples is insufficient for statistically significant statements about the role of these mutations in tumorigenesis. Nevertheless, these results and the prevalence of mutations in indirectly-contributing Ang2 residues suggest that the role of mutations in core or buried Ang2 residues in cancer should be investigated in future studies.

For a wider perspective, we applied our computational analysis to the SCF-c-Kit and M-CSF-c-FMS complexes and compared them to previous random mutagenesis and YSD screening.[32,36] Our comparison shows that our combined approach rapidly classified which RTK ligand residues contribute to receptor binding directly and which residues are sufficiently buried in the protein core to affect binding indirectly upon mutagenesis. This analysis also highlights that for RTK ligands that require dimerization for receptor activation, prediction of ligand residues that contribute directly to dimer formation is necessary for an accurate and comprehensive classification. Furthermore, the N430S variant of Ang2, which presumably affected Ang2 tertiary structure via perturbation of a metal binding site, shows that incorporating additional orthogonal computational approaches that predict such structural motifs (eg, Ref. 44), will further increase the coverage (reduce the false negatives) of combined prediction schemes.

From a more methodological point of view, our combined approach provides a rapid, accurate, and comprehensive way to interrogate the binding of protein ligands to their RTK receptors. Compared to a widely used knowledge-based method such as FOLD-X,[26,57] our approach provided more accurate predictions with fewer false-negatives and false-positives, while also adding information on the type of energy contributions, which can be used to better engineer this interface. A comparison to the sequence-based approach ISIS showed that most of the residues predicted by ISIS were far away from the interface with Tie2, while only very few of the residues actually involved in Tie2 binding were predicted by this method. Given that this is a sequence-based approach, this comparison highlights the advantages of using structure-based analysis when a structure of the complex is available. Alternatively, the simplicity and transparency of our physics-based computational classifications enable a more straight-forward integration with high-throughput screening methods such as YSD-using visual inspection of the complex structures. Obviously, burial-based predictions are not sufficient to predict which substitutions actually affect ligand-receptor binding indirectly; this limitation is addressed by the combination with high-throughput experimental screening. Compared to an exclusive use of high-throughput experimental methods, our computational approach provides a useful postscreening step that can reduce laborious and time-consuming work, while also providing a mechanistic and transparent explanation for the variants that are identified experimentally.

In summary, our validated residue-level map enables precise re-engineering of Ang2 to prevent binding to Tie2 towards potential therapeutics. Our study also provides a proof-of-concept for combining continuum-electrostatic and burial-based approaches with high-throughput mutagenesis and YSD by interrogating the residue-level determinants of Ang2 binding to Tie2. The analysis of the Ang2-Tie2, c-Kit-SCF and M-CSF-c-FMS complexes suggests that combining these physics-based computational methods with orthogonal computational predictions (such as sequence or structure knowledge-based methods) can better interrogate protein-protein interactions of additional RTKs and their ligands at the individual residue level.

ACKNOWLEDGMENTS

This work was supported by the European Research Council "Ideas program" ERC-2013-StG (contract grant number: 336041) to Niv Papo. Mickey Kosloff acknowledges support by grants from the Israel Science Foundation (grant numbers 1454/13, 1959/13, 2155/15) and from the Israel Ministry of Science, Technology and Space, Israel, and the Italian Ministry of Foreign Affairs (3-10704). The authors thank Emmanuel Levy and Rachel Kolodny for helpful discussions and comments.

AUTHOR CONTRIBUTIONS

Conceived and designed experiments: Anna Bakhman, Eitan Rabinovich, Tomer Shlamkovich, Niv Papo, Mickey Kosloff

Performed experiments: Anna Bakhman, Eitan Rabinovich, Tomer Shlamkovich

Analyzed data: Anna Bakhman, Eitan Rabinovich, Tomer Shlamkovich, Niv Papo, Mickey Kosloff

Wrote original manuscript draft: Anna Bakhman, Mickey Kosloff

Reviewed and edited manuscript: Anna Bakhman, Eitan Rabinovich, Tomer Shlamkovich, Niv Papo, Mickey Kosloff

ORCID

Niv Papo https://orcid.org/0000-0002-7056-2418
Mickey Kosloff https://orcid.org/0000-0003-1807-4000

REFERENCES

1. Gale NW, Thurston G, Hackett SF, et al. Angiopoietin-2 is required for postnatal angiogenesis and lymphatic patterning, and only the latter role is rescued by Angiopoietin-1. *Dev Cell*. 2002;3(3):411-423.
2. Eklund L, Olsen BR. Tie receptors and their angiopoietin ligands are context-dependent regulators of vascular remodeling. *Exp Cell Res*. 2006;312(5):630-641.
3. Benest AV, Kruse K, Savant S, et al. Angiopoietin-2 is critical for cytokine-induced vascular leakage. *PLoS one*. 2013;8(8):e70459.
4. Maisonpierre PC, Suri C, Jones PF, et al. Angiopoietin-2, a natural antagonist for Tie2 that disrupts in vivo angiogenesis. *Science*. 1997;277(5322):55-60.
5. Kim I, Kim JH, Moon SO, Kwak HJ, Kim NG, Koh GY. Angiopoietin-2 at high concentration can enhance endothelial cell survival through the phosphatidylinositol 3′-kinase/Akt signal transduction pathway. *Oncogene*. 2000;19(39):4549-4552.
6. Fiedler U, Krissl T, Koidl S, et al. Angiopoietin-1 and angiopoietin-2 share the same binding domains in the tie-2 receptor involving the first Ig-like loop and the epidermal growth factor-like repeats. *J Biol Chem*. 2003;278(3):1721-1727.
7. Yuan HT, Khankin EV, Karumanchi SA, Parikh SM. Angiopoietin 2 is a partial agonist/antagonist of Tie2 signaling in the endothelium. *Mol Cell Biol*. 2009;29(8):2011-2022.
8. Fiedler U, Reiss Y, Scharpfenecker M, et al. Angiopoietin-2 sensitizes endothelial cells to TNF-alpha and has a crucial role in the induction of inflammation. *Nat Med*. 2006;12(2):235-239.
9. Saharinen P, Eklund L, Pulkki K, Bono P, Alitalo K. VEGF and angiopoietin signaling in tumor angiogenesis and metastasis. *Trends Mol Med*. 2011;17(7):347-362.
10. Scholz A, Plate KH, Reiss Y. Angiopoietin-2: a multifaceted cytokine that functions in both angiogenesis and inflammation. *Ann N Y Acad Sci*. 2015;1347:45-51.
11. Gerald D, Chintharlapalli S, Augustin HG, Benjamin LE. Angiopoietin-2: an attractive target for improved antiangiogenic tumor therapy. *Cancer Res*. 2013;73(6):1649-1657.
12. Rosenfeld PJ, Brown DM, Heier JS, et al. Ranibizumab for neovascular age-related macular degeneration. *N Engl J Med*. 2006;355(14):1419-1431.
13. Ferrara N, Adamis AP. Ten years of anti-vascular endothelial growth factor therapy. *Nat Rev Drug Discov*. 2016;15(6):385-403.
14. Shlamkovich T, Aharon L, Barton WA, Papo N. Utilizing combinatorial engineering to develop Tie2 targeting antagonistic angiopoetin-2 ligands as candidates for anti-angiogenesis therapy. *Oncotarget*. 2017;8(20):33571-33585.
15. Saharinen P, Eklund L, Alitalo K. Therapeutic targeting of the angiopoietin-TIE pathway. *Nat Rev Drug Discov*. 2017;16(9):635-661.
16. Barton WA, Dalton AC, Seegar TC, Himanen JP, Nikolov DB. Tie2 and Eph receptor tyrosine kinase activation and signaling. *Cold Spring Harb Perspect Biol*. 2014;6(3):a009142.
17. Barton WA, Tzvetkova-Robev D, Miranda EP, et al. Crystal structures of the Tie2 receptor ectodomain and the angiopoietin-2-Tie2 complex. *Nat Struct Mol Biol*. 2006;13(6):524-532.
18. Barton WA, Tzvetkova D, Nikolov DB. Structure of the angiopoietin-2 receptor binding domain and identification of surfaces involved in Tie2 recognition. *Structure*. 2005;13(5):825-832.
19. Davis S, Aldrich TH, Jones PF, et al. Isolation of angiopoietin-1, a ligand for the TIE2 receptor, by secretion-trap expression cloning. *Cell*. 1996;87(7):1161-1169.
20. Valenzuela DM, Griffiths JA, Rojas J, et al. Angiopoietins 3 and 4: diverging gene counterparts in mice and humans. *Proc Natl Acad Sci U S A*. 1999;96(5):1904-1909.
21. Alber T. Mutational effects on protein stability. *Annu Rev Biochem*. 1989;58:765-798.
22. Serrano L, Kellis JT Jr, Cann P, Matouschek A, Fersht AR. The folding of an enzyme. II. Substructure of barnase and the contribution of different interactions to protein stability. *J Mol Biol*. 1992;224(3):783-804.
23. Matthews BW. Structural and genetic analysis of protein stability. *Annu Rev Biochem*. 1993;62:139-160.
24. Milla ME, Brown BM, Sauer RT. Protein stability effects of a complete set of alanine substitutions in arc repressor. *Nat Struct Biol*. 1994;1(8):518-523.
25. Wang Z, Moult J. SNPs, protein structure, and disease. *Hum Mutat*. 2001;17(4):263-270.
26. Guerois R, Nielsen JE, Serrano L. Predicting changes in the stability of proteins and protein complexes: a study of more than 1000 mutations. *J Mol Biol*. 2002;320(2):369-387.
27. Yue P, Li Z, Moult J. Loss of protein structure stability as a major causative factor in monogenic disease. *J Mol Biol*. 2005;353(2):459-473.
28. Moreira IS, Fernandes PA, Ramos MJ. Hot spot occlusion from bulk water: a comprehensive study of the complex between the lysozyme HEL and the antibody FVD1.3. *J Phys Chem B*. 2007;111(10):2697-2706.
29. Laskowski RA, Thornton JM. Understanding the molecular machinery of genetics through 3D structures. *Nat Rev Genet*. 2008;9(2):141-151.
30. Vishwanath S, Sukhwal A, Sowdhamini R, Srinivasan N. Specificity and stability of transient protein-protein interactions. *Curr Opin Struct Biol*. 2017;44:77-86.
31. Gai SA, Wittrup KD. Yeast surface display for protein engineering and characterization. *Curr Opin Struct Biol*. 2007;17(4):467-473.
32. Rabinovich E, Heyne M, Bakhman A, Kosloff M, Shifman JM, Papo N. Identifying residues that determine SCF molecular-level interactions through a combination of experimental and in silico analyses. *J Mol Biol*. 2017;429(1):97-114.
33. Rosenfeld L, Shirian J, Zur Y, Levaot N, Shifman JM, Papo N. Combinatorial and computational approaches to identify interactions of macrophage Colony-stimulating Factor (M-CSF) and its receptor c-FMS. *J Biol Chem*. 2015;290(43):26180-26193.
34. Yuzawa S, Opatowsky Y, Zhang Z, Mandiyan V, Lax I, Schlessinger J. Structural basis for activation of the receptor tyrosine kinase KIT by stem cell factor. *Cell*. 2007;130(2):323-334.
35. Chen X, Liu H, Focia PJ, Shim AH, He X. Structure of macrophage colony stimulating factor bound to FMS: diverse signaling assemblies of class III receptor tyrosine kinases. *Proc Natl Acad Sci U S A*. 2008;105(47):18267-18272.
36. Zur Y, Rosenfeld L, Bakhman A, et al. Engineering a monomeric variant of macrophage colony-stimulating factor (M-CSF) that antagonizes the c-FMS receptor. *Biochem J*. 2017;474(15):2601-2617.
37. Kosloff M, Travis AM, Bosch DE, Siderovski DP, Arshavsky VY. Integrating energy calculations with functional assays to decipher the specificity of G protein-RGS protein interactions. *Nat Struct Mol Biol*. 2011;18(7):846-853.
38. Asli A, Sadiya I, Avital-Shacham M, Kosloff M. "Disruptor" residues in the regulator of G protein signaling (RGS) R12 subfamily attenuate the inactivation of Galpha subunits. *Sci Signal*. 2018;11(534):eaan3677.
39. Kasom M, Gharra S, Sadiya I, Avital-Shacham M, Kosloff M. Interplay between negative and positive design elements in Galpha helical domains of G proteins determines interaction specificity toward RGS2. *Biochem J*. 2018;475(14):2293-2304.
40. Salem-Mansour D, Asli A, Avital-Shacham M, Kosloff M. Structural motifs in the RGS RZ subfamily combine to attenuate interactions with Galpha subunits. *Biochem Biophys Res Commun*. 2018;503(4):2736-2741.
41. Honig B, Nicholls A. Classical electrostatics in biology and chemistry. *Science*. 1995;268(5214):1144-1149.
42. Sheinerman FB, Al-Lazikani B, Honig B. Sequence, structure and energetic determinants of phosphopeptide selectivity of SH2 domains. *J Mol Biol*. 2003;334(4):823-841.
43. Nicholls A, Sharp KA, Honig B. Protein folding and association: insights from the interfacial and thermodynamic properties of hydrocarbons. *Proteins*. 1991;11(4):281-296.

44. Schymkowitz JW, Rousseau F, Martins IC, Ferkinghoff-Borg J, Stricher F, Serrano L. Prediction of water and metal binding sites and their affinities by using the fold-X force field. *Proc Natl Acad Sci U S A*. 2005;102(29):10147-10152.
45. Tokuriki N, Stricher F, Serrano L, Tawfik DS. How protein stability and new functions trade off. *PLoS Comput Biol*. 2008;4(2):e1000002.
46. Tien MZ, Meyer AG, Sydykova DK, Spielman SJ, Wilke CO. Maximum allowed solvent accessibilites of residues in proteins. *PLoS one*. 2013; 8(11):e80635.
47. Rose GD, Geselowitz AR, Lesser GJ, Lee RH, Zehfus MH. Hydrophobicity of amino acid residues in globular proteins. *Science*. 1985; 229(4716):834-838.
48. Miller S, Janin J, Lesk AM, Chothia C. Interior and surface of monomeric proteins. *J Mol Biol*. 1987;196(3):641-656.
49. Chao G, Cochran JR, Wittrup KD. Fine epitope mapping of anti-epidermal growth factor receptor antibodies through random mutagenesis and yeast surface display. *J Mol Biol*. 2004;342(2):539-550.
50. Cochran JR, Kim YS, Olsen MJ, Bhandari R, Wittrup KD. Domain-level antibody epitope mapping through yeast surface display of epidermal growth factor receptor fragments. *J Immunol Methods*. 2004;287(1–2): 147-158.
51. Tokuriki N, Stricher F, Schymkowitz J, Serrano L, Tawfik DS. The stability effects of protein mutations appear to be universally distributed. *J Mol Biol*. 2007;369(5):1318-1332.
52. Rost B, Sander C. Conservation and prediction of solvent accessibility in protein families. *Proteins*. 1994;20(3):216-226.
53. Pollastri G, Baldi P, Fariselli P, Casadio R. Prediction of coordination number and relative solvent accessibility in proteins. *Proteins*. 2002; 47(2):142-153.
54. Levy ED. A simple definition of structural regions in proteins and its use in analyzing interface evolution. *J Mol Biol*. 2010;403(4):660-670.
55. Ofran Y, Rost B. ISIS: interaction sites identified from sequence. *Bioinformatics*. 2007;23(2):e13-e16.
56. Yachdav G, Kloppmann E, Kajan L, et al. PredictProtein--an open resource for online prediction of protein structural and functional features. *Nucleic Acids Res*. 2014;42(Web Server issue):W337-W343.
57. Das R, Baker D. Macromolecular modeling with rosetta. *Annu Rev Biochem*. 2008;77:363-382.

SUPPORTING INFORMATION

Additional supporting information may be found online in the Supporting Information section at the end of the article.

How to cite this article: Bakhman A, Rabinovich E, Shlamkovich T, Papo N, Kosloff M. Residue-level determinants of angiopoietin-2 interactions with its receptor Tie2. *Proteins*. 2019;87:185–197. https://doi.org/10.1002/prot.25638